nature communications

Article

https://doi.org/10.1038/s41467-025-65981-9

Magnetic reconnection in the plasma disk at 23 Jupiter radii

Received: 11 April 2025

Accepted: 27 October 2025

Published online: 10 December 2025

Check for updates

Jian-zhao Wang[1,2] ✉, Fran Bagenal[1], Stefan Eriksson[1], Robert E. Ergun[1,2], Peter A. Delamere[3], Robert J. Wilson[1], Robert W. Ebert[4,5], Philip W. Valek[4], Frederic Allegrini[4,5] & Licia C. Ray[6]

A key open question in astrophysics is how plasma is transported within strongly magnetized, rapidly rotating systems. Magnetic reconnection and flux tube interchange are possible mechanisms, with Jupiter serving as the best local analog for distant systems. However, magnetic reconnection at Jupiter remains poorly understood. A key indicator of active magnetic reconnection is the ion diffusion region, but its detection at Jupiter had not been confirmed previously. Here, we report a magnetic reconnection event in Jupiter's inner magnetosphere that presents the detection of an ion diffusion region. We provide evidence that this event involves localized flux tube interchange motion driven by centrifugal forces, which occurs inside a thin current sheet formed by the collision and twisting of two distinct flux tubes. This study provides insights into Io-genic plasma transport at Jupiter and the unique role of magnetic reconnection in rapidly rotating systems, two key unresolved questions.

Centrifugal forces play a significant role in structuring the Jovian magnetosphere, which is characterized by its strong intrinsic magnetic field, an internal plasma source from Io's escaping atmosphere, and fast planetary rotation[1]. As a crucial aspect of the system's dynamics, magnetic reconnection is believed to be a key mechanism in governing plasma behavior. At Jupiter, magnetic reconnection features a dominance of heavy ions, possible corotating reconnection sites in a strong magnetic field[2], and radial stress driven by centrifugal forces[3], making it distinct from reconnection at Earth or other magnetized planets. In the outer region beyond 30 R_J (R_J = 71,492 km is Jupiter's equatorial radius), weakened magnetic fields are stretched as plasma moves outward due to centrifugal forces. Ultimately, magnetic reconnection may occur at an intersection of opposing magnetic field lines, leading to the pinching off of plasmoids, as part of the Vasyliūnas cycle[4].

The Io-genic plasma is transported outward and confined near the equator under centrifugal forcing, forming a plasma disk[5]. In the inner region within 30 R_J, radial plasma transport is thought to be facilitated by flux tube interchange, which occurs spontaneously when the flux tube content decreases radially[6,7]. It is difficult to fully interchange whole tubes through ionospheric convection because the equatorial region, which contains most of the plasma, is more unstable than the latitudinal regions. X. Ma et al. [8] proposed a localized process that exchanges part of neighboring flux tubes through equatorial plasma flow convection. As the convection progresses, the off-equatorial regions are dragged and twisted, forming a pair of reconnection sites triggered by antiparallel magnetic components[9]. This mechanism, known as localized flux tube interchange driven magnetic reconnection, could efficiently facilitate the outward transport of Io-genic plasma, although no direct observational evidence has been found to date.

Magnetic reconnection in the Jovian system is typically proposed from its observable byproducts, e.g., flux ropes, plasmoids, and dipolarization fronts[10–13]. Near the magnetic X-line of reconnection, ions decouple from the magnetic field, introducing an ion diffusion region with the presence of a quadrupole Hall magnetic field, which serves as a key indicator of local reconnection first observed at

[1]Laboratory for Atmospheric and Space Physics, University of Colorado Boulder, Boulder, CO, USA. [2]Department of Astrophysical and Planetary Sciences, University of Colorado Boulder, Boulder, CO, USA. [3]Geophysical Institute, University of Alaska Fairbanks, Fairbanks, AK, USA. [4]Southwest Research Institute, San Antonio, TX, USA. [5]Department of Physics and Astronomy, University of Texas at San Antonio, San Antonio, TX, USA. [6]Physics Department, Lancaster University, Lancaster, UK. ✉e-mail: jiwa1124@colorado.edu

Earth[14–17] and also identified at other planets[18–21]. The Hall field is generated as electrons stream along the separatrix regions toward the X-line and jet away from the X-line in two reconnection outflow regions. The ion diffusion region has remained undetected at Jupiter due to its small scale and dearth of high-quality plasma data. The polar-orbiting Juno spacecraft around Jupiter enables the high-cadence off-equator measurements to address whether flux tube interchange reconnection can proceed close to the planet as theorized.

In this work, we present the detection of ion diffusion region at Jupiter in support of a flux tube interchange driven reconnection inside 30 R_J. As the innermost reconnection event ever observed at Jupiter, this event is triggered by compression between two interlaced flux tubes with distinct properties, with a thin current sheet forming between them. The evidence includes the presence of a Hall magnetic field with a guide field, ion plasma acceleration consistent with the Walén relation, and plasma pitch-angle distributions that reveal plasma energization. Coincidentally, the event also exhibits a pair of twisted flux tubes located symmetrically about the equator—strong evidence of the developing localized flux tube interchange. This study illustrates the distinct reconnection mechanism operating in the inner Jovian system and how Io-genic plasma is transported through localized interchange processes.

Results

Overview of the magnetic reconnection event

An overview of the event is shown in Fig. 1. The magnetic field is measured by the MAG instrument[22], and the plasma parameters are obtained using a forward modeling method[23,24] based on thermal plasma data from the JADE instrument[25]. All observations are presented in the Jupiter-De-Spun-Sun (JSS) coordinate system. In spherical coordinates, near the equator, the r, θ, and ϕ components approximate to the radial direction, the north-to-south direction aligned with Jupiter's spin axis, and the bulk velocity direction of plasma corotating with Jupiter, respectively. As illustrated in Fig. 1b, c, this event occurred at a radial distance of 23.3 R_J and a local time of 22.6 h, near the midnight magnetic equator, on July 24, 2020. The event lies within the plasma disk, far from both the magnetopause[26] and the statistical magnetic reconnection X-line driven by the Vasyliūnas cycle, as identified by Galileo observations[10]. This location within the inner magnetosphere does not support mechanisms involving magnetosheath reconnection or reconnection driven by the Vasyliūnas cycle.

In Fig. 1d, B_r shifts from negative to positive, indicating that Juno was crossing the plasma disk at 01:55 UT, where B_r is about 0, from south to north. Around this crossing, typical plasma disk features are observed, including a strong, stable B_θ and a plasma flow reaching 80% of the rigid corotational velocity (v_ϕ is about 235 km/s)[24,27]. South of the equator, Juno detects a structure with entangled flux tubes, characterized by its helical magnetic field (Fig. 1e) and a sharp density contrast between the two tubes (Fig. 1f). The first half of the structure features a tenuous, hot flux tube with increased B_θ that indicates inward stretching, while the second half contains a dense, cold flux tube with decreased B_θ that indicates outward stretching. The opposite trend in B_ϕ indicates that the two tubes are twisted around each other.

On the north side of the equator, Juno detects evidence of a magnetic reconnection event. First, B_θ increases sharply after a brief negative dip, rising from −9 nT to 43 nT in 20 s (Fig. 1e). This increase is 4.4 times greater than the average rise amplitude and 76% shorter than the median rise time of dipolarization fronts reported by Blöcker et al. [13]. Simultaneously, B_ϕ decreases from 40 nT to 10 nT. The rapid changes in both B_ϕ and B_θ suggest the presence of an intense and very thin current sheet where reconnection could potentially occur. The shear angle between the magnetic fields on opposite sides of the current sheet is 86.2 deg., which is sufficient to trigger magnetic reconnection, as observed at Jupiter (e.g., Montgomery et al.[28]) and Earth (e.g., Kacem et al.[29]). Second, both electron and ion data show a similar trend, with a dense, cold flux tube and a tenuous, hot flux tube closely located on opposite sides of the current sheet (Fig. 1j to Fig. 1m). Consistent with the southern structure, B_θ increases in the tenuous tube and decreases in the dense tube, but with greater variation, indicating that the two tubes are compressed against each other. This suggests that magnetic reconnection could occur within the thin current sheet formed at the center of two compressed, interlaced flux tubes (discussed further below). Plasma flow is also accelerated in the θ direction by about 100 km/s (Fig. 1n). The Alfvén speed is calculated to be 91 km/s, which closely matches the increase in flow velocity, showing consistency between the observations and the Walén relation[30]. Additionally, the input magnetic energy density of 6.7×10^{-10} J/m^3 aligns with a plasma kinetic energy density gain of 8.0×10^{-10} J/m^3 (see the "Methods" section, subsection "Estimations of Key Parameters in the Magnetic Reconnection Event", for details), demonstrating consistency with the principle of energy conservation in magnetic reconnection. Third, pitch angle distributions (PADs) reveal that while electrons remain field-aligned (Fig. 1i), ions exhibit an asymmetric PAD (Fig. 1h). Prior to the current sheet, ions predominantly stream near 0°, whereas following the current sheet, ion flux is enhanced near 180°. Differences in the PADs of ions and electrons indicate decoupling between the two species. Finally, after reconnection, harmonic plasma waves near the local electron plasma frequency (f_{pe}) and its second harmonic ($2f_{pe}$) are observed by Juno's WAVES instrument[31] on the low-density side (see Supplementary Fig. 1 for details). These waves may be generated by nonlinear interactions between the reconnection flows and the ambient plasma[32]. In summary, the observations of magnetic fields, plasma bulk flow parameters, PADs, and plasma waves are consistent with the detection of a reconnection event.

Considering the southern entangled flux tubes structure and the northern reconnection event together, these observations suggest a localized interchange driven reconnection process, supported by multiple lines of evidence. First, this event occurred at a radial distance of 23.3 R_J, which is near the outer boundary of observed interchange events[33] but significantly closer to Jupiter than the expected locations of Vasyliūnas cycle driven reconnection events[34]. Unlike whole flux tube interchange, partial and localized interchange is expected at this location due to the weakened magnetic field[9]. Second, the two regions are symmetrically located with respect to the equator, where each interval of decreased B_θ contains a dense, cold flux tube, and each interval of increased B_θ contains a tenuous, hot flux tube. Quantitatively, the entangled tubes structure and reconnection event are located 0.39 R_J south and 0.33 R_J north of the plasma disk center, respectively. The observations also suggest the twisting of two flux tubes related to interchange, with the two highly correlated regions representing different stages of the process and observed by Juno at different times. The entangled tubes structure represents the early growth stage of twisting, where the magnetic field begins to distort. Approximately 15 min later, as Juno traveled from the southern to the northern disk, it encountered the corresponding magnetic reconnection site. Here, the field was strongly twisted, and magnetic reconnection was triggered by a sufficient shear angle. Third, the two regions exhibit opposite polarities in magnetic field and plasma parameters, consistent with localized interchange driven reconnection, which shears the magnetic fields of the paired sites in opposite directions. In the southern region, the dip in B_θ, along with a dense, cold flux tube, appeared in the second half. A similar signature was also observed in the northern region, but it occurred before the current sheet. The low B_θ magnitude could result from the radially stretched magnetic field during the mass-loaded flux tube's transport. Lastly, the flow is accelerated in the θ direction (discussed further below), contrasting with typical Vasyliūnas cycle driven reconnection signatures or plasma injection events[3,35], where radial-directed flows are expected.

https://doi.org/10.1038/s41467-025-65981-9

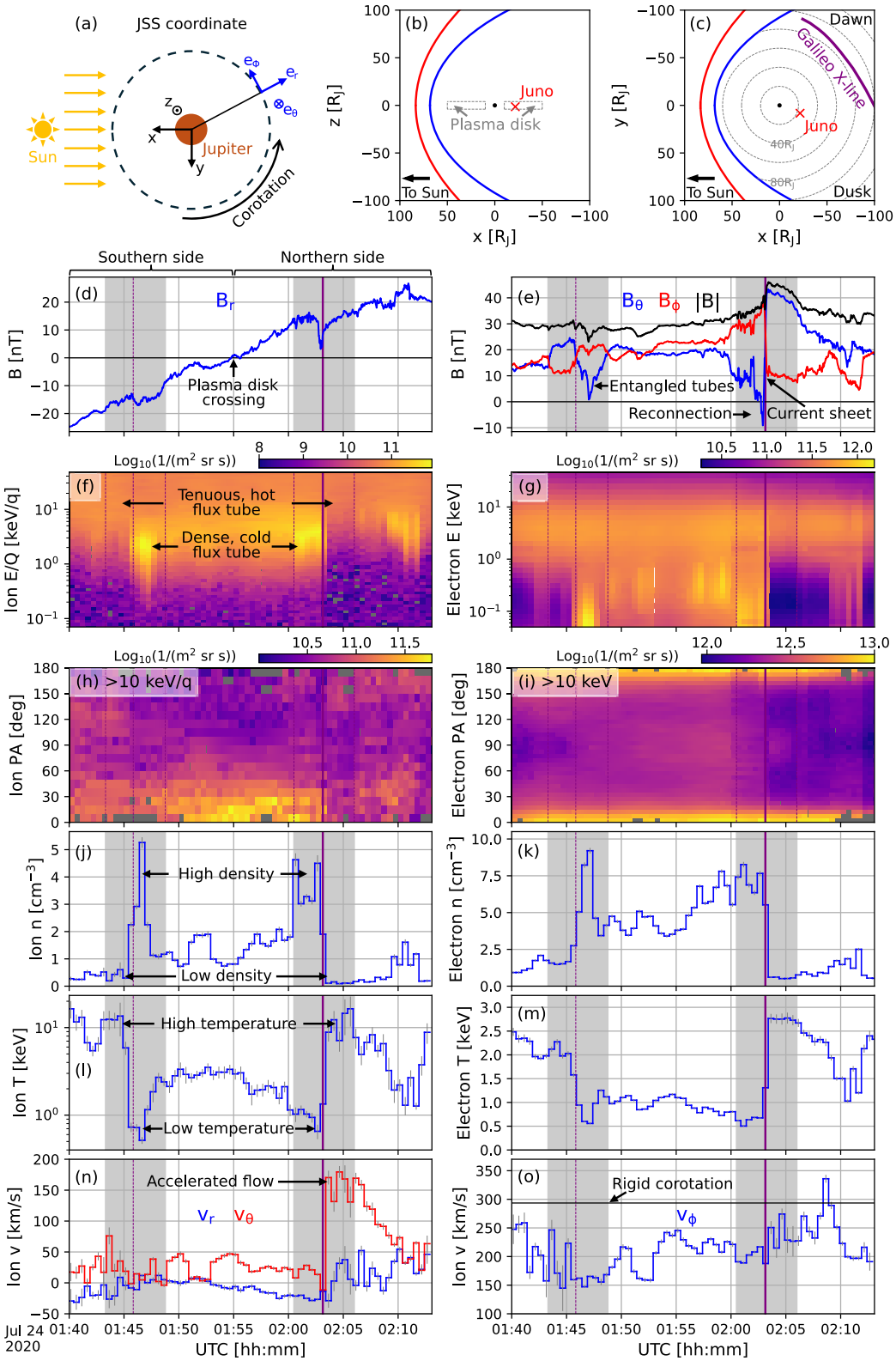

Fig. 1 | Overview of the magnetic reconnection event. a Illustration of the Jupiter-De-Spun-Sun (JSS) coordinate system near the equator, viewed from above the north pole, in which the observations are presented. **b**, **c** Event location in the inner magnetosphere; **d**, **e** magnetic field measurements from the MAG instrument; **f**, **g** heavy ion and electron flux spectra from the JADE instrument; **h**, **i** pitch angle (PA) distributions; **j**, **k** plasma densities (*n*); **l**, **m** plasma temperatures (*T*); and **n**, **o** plasma velocities (**v**). In certain panels, the left and right gray-shaded regions indicate the entangled flux tubes structure and the magnetic reconnection event, respectively, with the location of the current sheet marked by a thick, solid vertical purple line. The error bars represent ±1σ uncertainties in the plasma parameters. Source data are provided as a Source Data file.

https://doi.org/10.1038/s41467-025-65981-9

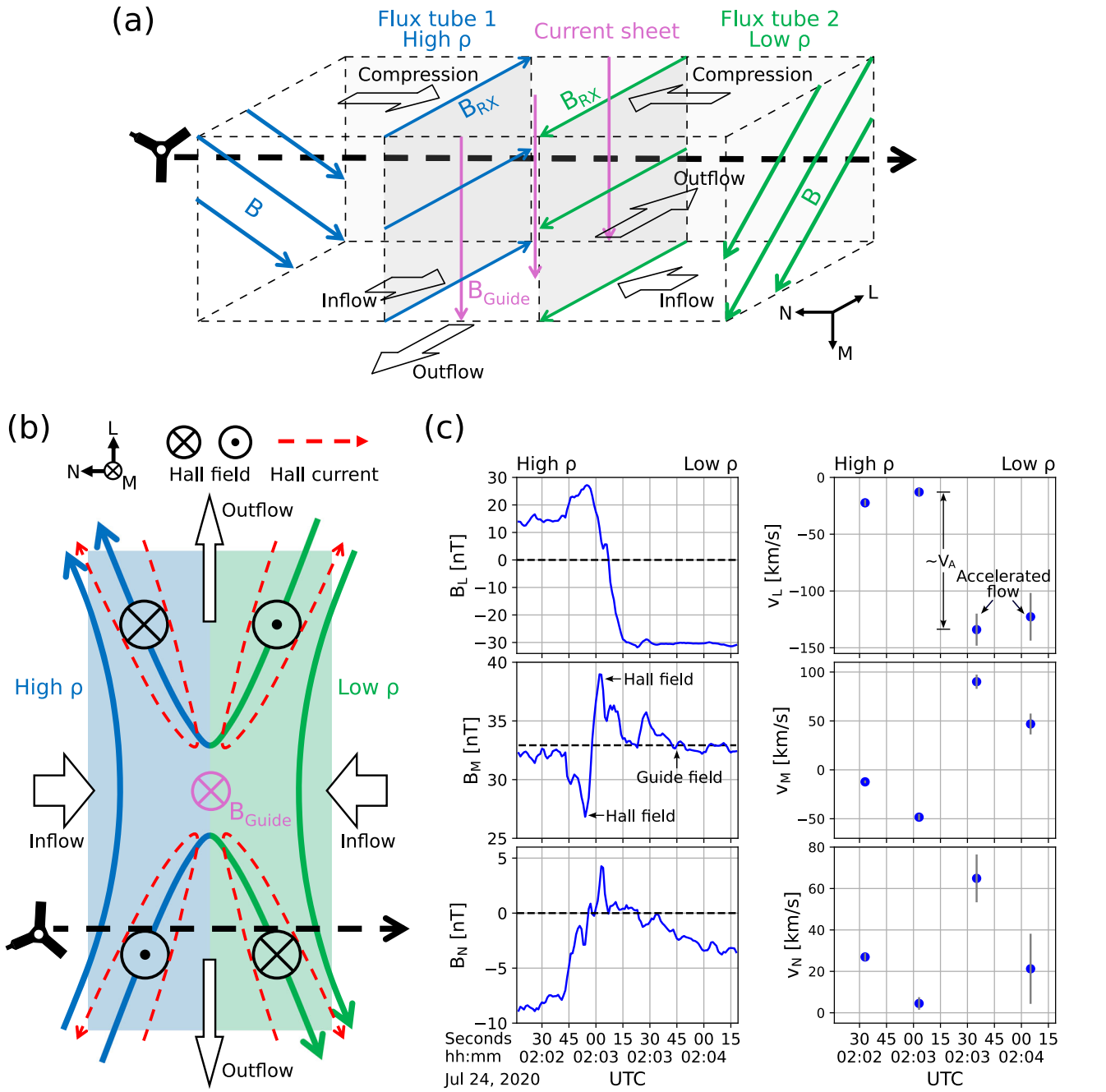

Fig. 2 | Overview of observations in the ion diffusion region (IDR). a Illustration of the magnetic reconnection event trigger mechanism. The event is driven by compression between two interlaced flux tubes, with a thin current sheet and guide field forming between them. B_{RX} and B_{Guide} are the reconnecting and guide magnetic fields, respectively. **b** Illustration of the diffusion region and Juno's trajectory. Juno traverses the region from the high-density (high ρ) side to the low-density (low ρ) side, with a corresponding change in the Hall magnetic field direction. **c** Magnetic fields and plasma flows in the LMN coordinate system. The error bars represent ±1σ uncertainties in the plasma velocities. Juno is depicted by the spacecraft icon, and its trajectory is depicted as the dashed black line with an arrow. Source data are provided as a Source Data file.

Diffusion region observations

Figure 2a illustrates the mechanism triggering the magnetic reconnection event. Due to interchange motion driven by centrifugal forces, two interlaced flux tubes with distinct properties exert pressure on each other. This compression causes magnetic field pileup, leading to the formation of a thin current sheet between them. Consequently, the parallel components of the magnetic field in the two flux tubes correspond to a guide field (i.e., B_{Guide}), while the anti-parallel components (i.e., B_{RX}) facilitate magnetic reconnection, producing large-scale Alfvénic ion flow. Juno traverses the current sheet from the high-density side to the low-density side, consistent with an asymmetric reconnection event characterized by a magnetic field shear angle of 86 deg. and a density gradient. Similar reconnection events in thin current sheets have been observed in Earth's magnetosphere[29,36–39].

To investigate the diffusion region in the thin current sheet, the observations are re-organized in the local current sheet LMN coordinate system[40,41] (see the "Methods" section, subsection "Determination of the LMN Coordinate System", for details). As illustrated in Fig. 2b, near the X-line of magnetic reconnection, the N-direction is normal to the current sheet, the M-direction aligns with the Hall magnetic field, and the L-direction represents the outflow direction. As shown in

Fig. 2c, the B_L component changes from positive to negative, reflecting the sharp magnetic field rotation as Juno traverses from one side of the thin current sheet to the other. The Hall quadrupolar magnetic field, identified by the bipolar reversal in B_M, provides direct evidence of the detected ion diffusion region, while a background of 33 nT in the B_M profile suggests a substantial guide field. The $\triangle B_M < 0$ lobe of the bipolar B_M pattern is 'shunted away' from the current sheet center (where B_L is zero) and the $\triangle B_M > 0$ lobe covers a wider part of the exhaust region, consistent with the guide field asymmetry effect on the Hall field[42].

The plasma flow velocities in the LMN system are presented in the co-rotating frame (Fig. 2c), converted from velocities in the JSS system under the assumption that the reconnection site co-rotates with the planet. Plasma acceleration resulting from magnetic reconnection is observed in the low-density flux tube region, with accelerated velocities primarily in the negative L-direction, consistent with the proposed trajectory. The maximum v_L flow is offset from the current sheet center toward the low-density side, which is expected in reconnection with high density asymmetry[29,43–45]. The plasma is also accelerated in the M-direction, which may be associated with the planet exerting a force that more easily pulls on the recently reconnected, low-density field lines, as the M-direction roughly aligns with Jupiter's rotation. The highly twisted magnetic topology, relatively strong magnetization, and the distance from the X-line may also contribute to the flow deflection. Quantitatively, the ion inertial length, $d_i = c/\omega_{pi}$, is estimated to be 370 km. Juno traverses the current sheet in 25 s, defined as the time interval between the positive and negative maxima of B_L. Neglecting Juno's motion and assuming a flow along the normal to the current sheet at an average v_N of about 29 km/s (Fig. 2c), this corresponds to a normal width of 725 km or approximately 2 d_i.

Figure 3a shows the energy-dependent PADs of thermal electrons from JADE and energetic electrons from JEDI[46]. In addition to data from the dense tube and low-density tube regions of the magnetic reconnection event, observations from a separate plasma disk crossing at 21 R_J are included for comparison as representative of typical background conditions without significant perturbation. This crossing occurred about four hours after the reconnection event on the same day. Figure 3b shows the PADs at three selected energy levels. In the background plasma, electrons exhibit field-aligned distributions across all energies, consistent with typical regions outside 15 R_J in the absence of magnetic reconnection[47]. In contrast, the dense tube region shows a broader energy spectrum, while electron fluxes below 1 keV in the low-density tube are significantly depleted after the magnetic reconnection. In both regions, electrons show symmetric PADs. Near the X-line of reconnection, asymmetric electron PADs are expected on timescales shorter than the electron bounce time. For example, the bounce time of a 1 keV electron is about 0.017 s in this case, which is much shorter than JADE's cadence, explaining why asymmetries are not observed in the electron PADs between the low- and high-density flux tubes. Additionally, an asymmetric electron PAD is expected in the electron diffusion region, which is tiny compared with the spacecraft's relatively fast motion. The instrument's dwell time in the region is insufficient to resolve electron PAD asymmetries.

In the low-density tube region, electron fluxes are enhanced near 90° pitch angles for energies above 10 keV. Electron energization is often observed in association with magnetic reconnection near the X-line[48–50]. Figure 3c shows the combined JADE and JEDI energy spectra for both regions, summed over all pitch angle bins. Differences between JADE and JEDI fluxes are reconciled to produce smooth spectra. The average spectrum at 25 R_J from Liu et al. [51] is also shown for comparison. Compared to the dense tube region, the low-density tube exhibits reduced fluxes at low energies, resulting in a much harder spectrum with a decreased spectral slope. This harder spectrum provides additional evidence of plasma energization by magnetic reconnection.

Conceptual diagram

Combining the southern entangled flux tubes and the northern current sheet, this study provides the observational evidence of magnetic reconnection driven by localized flux tube interchange in Jupiter's magnetosphere. As illustrated in Fig. 4, at t_1, the system becomes unstable under centrifugal force due to the configuration of an inner, mass-loaded flux tube and an outer, lower-mass flux tube. The inner tube, experiencing a larger centrifugal force, tends to exchange positions with the outer tube to achieve equilibrium. However, the exchange of two whole flux tubes is constrained by the requirement for the convection of their footprints in the ionosphere. Instead, the equatorial region is more unstable to centrifugal instability, leading to a localized interchange. During this process, the inner partial tube moves outward while the outer one moves inward, causing the two tubes to stretch relative to each other. Simultaneously, vortical flow convection occurs near the equator, twisting the magnetic field lines locally. Consequently, a pair of off-equator structures with entangled flux tubes forms at t_2, with Juno traversing the southern one during this period.

As the twisting and stretching motions intensify, magnetic reconnection is triggered at t_3 when the shear angle between the magnetic fields of the two flux tubes becomes sufficiently large with enough magnetic stresses across the thin layer. This results in the formation of a pair of off-equator reconnection sites, with Juno traversing the northern site at that time. The vertical plasma flows could be explained by the growth rate of the interchange mode in a rotating system, which depends on the Alfvén speed, as illustrated by Ferrière[52] and Achilleos et al.[1]. The higher the plasma density, the lower the Alfvén speed, and the easier it is for the magnetic field lines to bend. As a result, the inner flux tube undergoes stronger stretching and is more significantly distorted than the outer tube, causing the 'X-shape' within the dashed-line box of Fig. 4c to skew and produce northward/southward plasma flows. During the proposed asymmetric reconnection event, the outflow is primarily aligned with the vertical direction of the anti-parallel magnetic field components in the two flux tubes, as illustrated in the diagram. Following the reconnection, the two flux tubes merge, completing the localized interchange process at t_4. As a result, plasma originating from Io is transported outward, accompanied by the relaxation of the twisted flux tubes.

Discussion

As a primary indicator of magnetic reconnection, changes in magnetic field topology are supported by multiple lines of evidence. First, the rapid rotation and variation in B_θ and B_ϕ suggest a twisted flux tube structure. A sharp boundary at the center of this structure supports the presence of a thin current sheet. Second, in the LMN coordinate analysis, a clear reversal in B_L indicates that the spacecraft crossed the current sheet from one side to the other. The bipolar signature in B_M provides direct evidence of the Hall magnetic field within the diffusion region, characteristic of local magnetic reconnection.

The idea that the current sheet is introduced by compression between two flux tubes is inferred to be the most likely mechanism. In Fig. 1n, the dense tube before the current sheet shows negative v_r, and the tenuous tube after it shows positive v_r, indicating the two tubes are moving toward each other. We also examined the N-direction flow velocity (i.e., v_N) over a broader time range (see Supplementary Fig. 2). Apart from two measurements near the X-line, no large-scale converging flows are seen, possibly because the X-line is a highly localized structure that may rotate rapidly compared to the 6 min interval analyzed in Supplementary Fig. 2. Given the complex magnetic topology caused by stretching and twisting, the observations outside the diffusion region are not necessarily well organized in the local LMN coordinate system. Additionally, JADE's 30 s cadence limits resolution, and v_N, being much smaller than v_M and v_L, may not be accurately resolved through forward modeling. The reconnection accelerated

https://doi.org/10.1038/s41467-025-65981-9

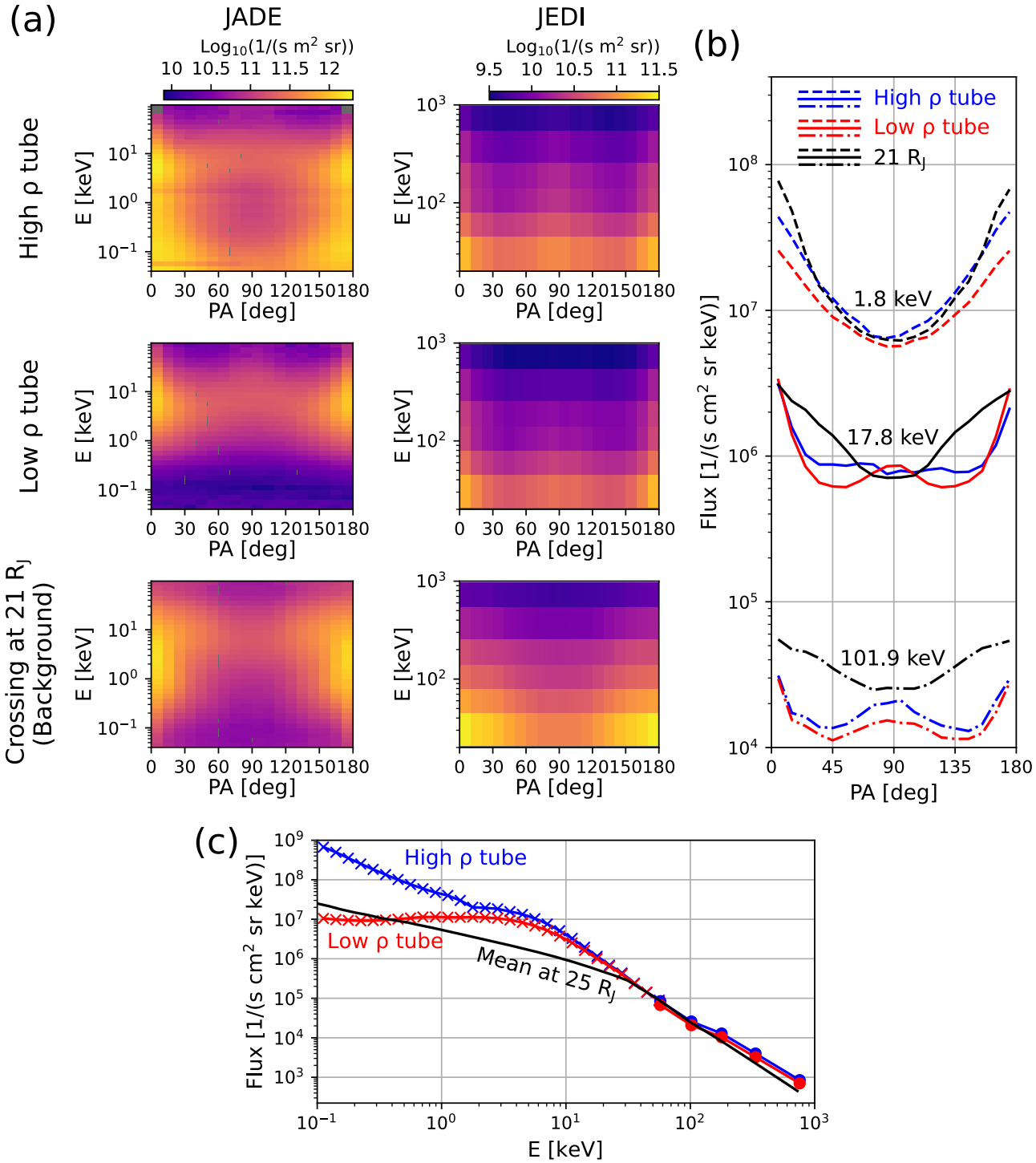

Fig. 3 | Electron plasma energization associated with the magnetic reconnection event. a, **b** Pitch angle (PA) distributions of electrons in the high-density (high ρ) tube region (02:00:42-02:02:42 UT) and low-density (low ρ) tube region (02:03:45-02:05:45 UT) of the magnetic reconnection event, along with a typical case at the plasma disk center at 21 R_J (05:55:00-06:03:00 UT). **c** Electron spectra in the high- and low-density tubes, compared with the mean spectrum at 25 R_J from Liu et al.[51]. Thermal and energetic electrons are detected by the JADE and JEDI instruments, respectively. Source data are provided as a Source Data file.

flow (i.e., v_L) is also examined over a broader time interval, as shown in Supplementary Fig. 3. The unusually large-scale flow, persisting for about 5 min, may be explained by several mechanisms. The strong density gradient across the current sheet may cause the flow to extend more into the low-density region, where lower inertia allows plasma to evacuate more efficiently and propagate farther. A moderate guide field can suppress turbulent mixing and promote well-directed, collimated reconnection flows that remain coherent over long distances.

We also examined the highest resolution plasma data available (see Supplementary Fig. 4) to search for a clear signature of a reconnection outflow, with a typical width of approximately d_i and a duration of a few seconds, possibly hidden within the large-scale flow structure. Within the identified diffusion region, an enhancement in electron density is observed, which is a signature of electron trapping by parallel electric field near the X-line[53]. As expected, the heavy ion signals peak every 30 s, reflecting JADE-I's once-per-spin sampling

https://doi.org/10.1038/s41467-025-65981-9

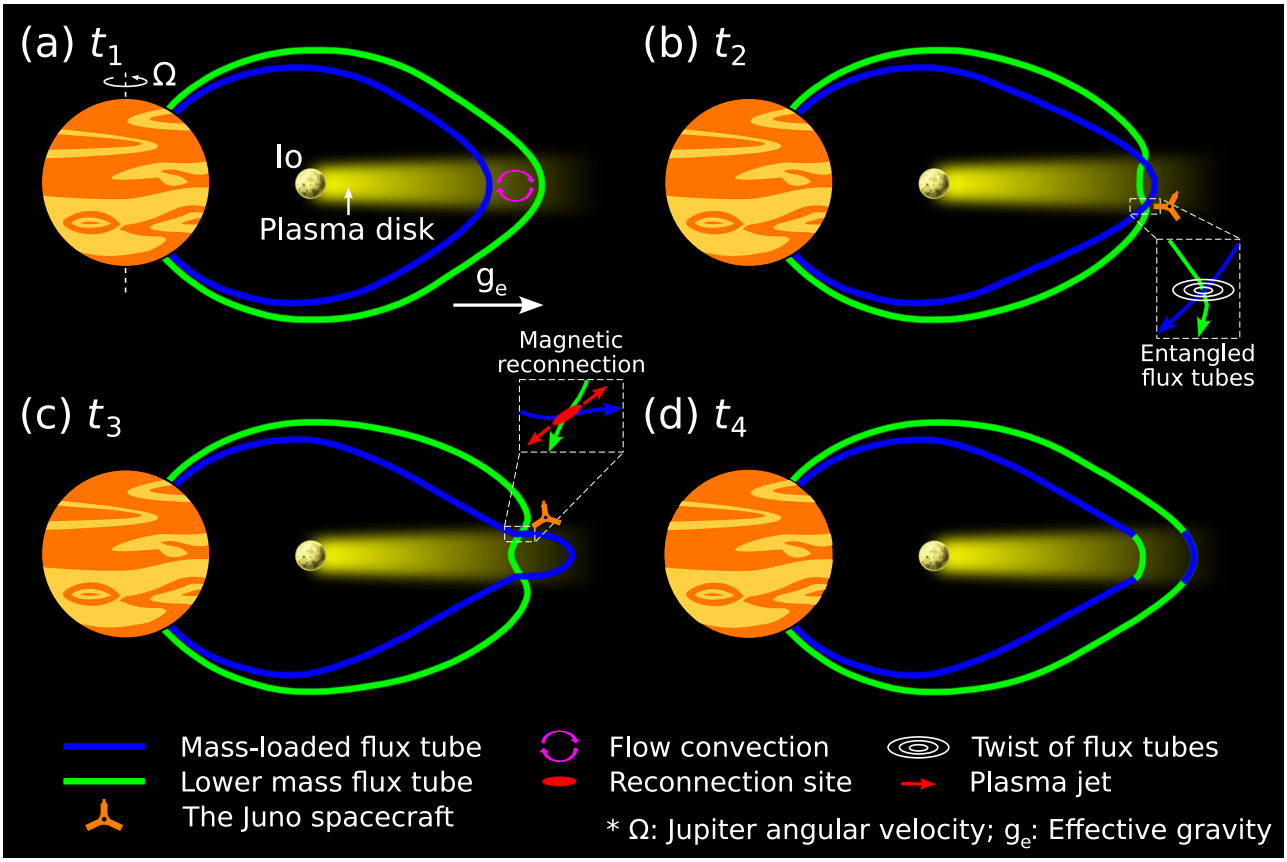

Fig. 4 | Simplified 2-D illustration of magnetic reconnection from localized flux tube interchange (not to scale). a The initial state at t_1. **b** Twisting of magnetic field lines with the formation of a pair of structures with entangled flux tubes at t_2. **c** Formation of a pair of reconnection sites at t_3. **d** Completion of the localized flux tube interchange at t_4. The effective gravity (g_e) is dominated by the centrifugal force.

cadence for ion flows. In comparison, after the diffusion region, the proton signals peak every 15 s, indicating bi-directional proton flows and the decoupling from heavy ions after reconnection. Unfortunately, Juno did not observe a narrow ion jet within the diffusion region. JADE has twelve 22.5° wide anodes, and at each time step, it samples only a small portion of the 4π steradian sky. Given the narrow spatial extent of the diffusion region, the JADE anodes are unlikely to observe the jet at the current sheet due to limitations in angular and temporal resolution. Another possible explanation for the missing narrow jet is the possible complex trajectory within the diffusion region. For example, if Juno followed the trajectory illustrated in Supplementary Fig. 5, it may not have traversed the outflow region but instead skimmed over it in an arch-shaped path, thereby missing the narrow jets in the diffusion region. We do not wish to overstate this event; therefore, the complex trajectory is not adopted here.

Moreover, we examined all 51 plasma disk crossings by Juno between 20 and 25 R_J. Many of these events exhibit small-scale, intermittent signatures accompanied by fluctuating magnetic fields. The alternating presence of hot, tenuous plasma and cold, dense plasma observed in these cases is a typical signature of flux tube interchange, the dominant plasma transport mechanism in this region. Among all the cases, only the event analyzed in this study shows a strong magnetic field signature characterized by entangled flux tubes, twisted magnetic field topology, and a thin current sheet—highlighting the uniqueness of this event. Given the prevalence of flux tube interchange in this region and the signatures in this particular case, we propose that it most likely represents a magnetic reconnection event driven by localized flux tube interchange.

Observations in this study suggest that localized interchange driven reconnection occurs within the plasma disk. In contrast, the simulation by Ma et al.[8] suggests 'high latitude' reconnection, due to their use of a uniform density profile along the z-direction, which is an artificial onset condition. In reality, most plasma content and centrifugal force are concentrated at low latitudes, as the density decreases exponentially away from the equator. The interchange instability is expected to be confined to the plasma disk. Additional simulations that incorporate more realistic conditions are needed for further investigation.

Some other mechanisms are considered unlikely. At 23.3 Jupiter radii, the plasma disk is generally expected to corotate with Jupiter with little perturbation. This much closer location, compared to the Galileo X-line, makes reconnection driven by the Vasyliūnas cycle unlikely. The observed vertically directed flows do not suggest inward plasma injections. Finally, this event occurred far from any of the Galilean moons, suggesting no influence from moon-plasma interactions.

In this study, we report strong evidence of a guide field magnetic reconnection event occurring at 23.3 Jupiter radii within the plasma disk, which is the innermost one observed in Jupiter's magnetosphere to date. It is also the compelling observation of an ion diffusion region resulting from magnetic reconnection at Jupiter, identified by the signature of the asymmetric Hall magnetic field. Ion plasma acceleration perpendicular to the equator is directly observed through thermal plasma measurements, with the accelerated flow offset toward the low-density side, likely due to significant density asymmetry. Additionally, the electron pitch angle distribution reveals plasma energization, characterized by a flux enhancement near 90 deg pitch angles and a harder spectrum after reconnection. Further verification is provided by examining the Walén relation, energy conservation, and the ion inertial scale, all of which show consistency with the observations.

This event is also the observational evidence of flux tube interchange driven reconnection at Jupiter, supported by its location deep within the magnetosphere, the observation of a pair of structures symmetrically located relative to the plasma disk equator with opposite magnetic field polarities, and the presence of clear signatures of magnetic reconnection, particularly in the local magnetic field configuration and particle fluxes. It demonstrates that interchange motion involves a complex build-up of twisted flux tubes, which are ultimately relaxed by reconnection. A thin current sheet is formed; a possible explanation is the collision between two flux tubes with distinct properties, driven by centrifugal force induced stretching and twisting. In this thin current sheet, asymmetric reconnection occurs, characterized by a large guide field and a significant density difference.

In the study of Jupiter's magnetosphere, two of the most important open questions are how magnetic reconnection governs the system and how Io-genic plasma is transported outward and ultimately lost. This study sheds light on both issues and helps refine models of Jovian magnetospheric dynamics. On the one hand, the proposed mechanism of localized flux tube interchange could play a crucial role in making the transport of Io-genic plasma more efficient. On the other hand, this study reveals key characteristics of interchange-driven magnetic reconnection, including the complex nature of twisted flux tubes merging, a reconnection scenario that previously lacked observational evidence. Magnetic reconnection is a key process in plasma physics, and these results offer valuable constraints for future simulations. Finally, this research offers a perspective on how magnetized plasmas behave in astrophysical systems with rapid rotation, strong magnetic fields, and massive plasma sources, e.g., giant planets, pulsars, brown dwarfs, and accretion disks. Since centrifugally driven localized processes could also occur in these systems, this study highlights its broader astrophysical significance.

Methods

Forward modeling of the thermal plasma data

Using data from the Juno/JADE ion detector (JADE-I), we employ a two-step forward modeling method to derive plasma parameters. Within one spacecraft spin, JADE-I measures ion count rates at different energy levels from multiple views and directions, covering 6 π steradians in High Rate Science mode and 4 π steradians in Low Rate Science mode (i.e., the SPECIES data). JADE-I also records accumulated count rates in different time-of-flight bands (i.e., the TOF data). In the first step, assuming the plasma follows the kappa distribution, we fit the TOF data to determine the abundances of five major ion species: O^+, O^{++}, S^+, S^{++}, and S^{+++}. In the TOF data, signals from O^+ and S^{++} overlap due to their similar mass-to-charge ratios. The density ratio between them is fixed as $n(O^+):n(S^{++}) = 1.2$, inferred from a physical chemistry model in Delamere et al.[54]. In the second step, with fixed ion abundances, we fit the SPECIES data to determine the plasma bulk parameters, including density (n), temperature (T), and 3-D bulk velocities ($\mathbf{v}$) in the Jupiter-centered Jupiter-De-Spun-Sun (JSS) coordinate system. The parameter n is the combined number density of five ion species with an average charge of 1.5. In the JSS system, the z-axis aligns with Jupiter's spin axis. The y-axis is defined as the cross product of $+z$ with the Jupiter-to-Sun vector. The x-axis completes the right-handed system and is approximately directed toward the Sun. Details of this forward modeling technique are elaborated in J. Wang et al.[23,24]. The forward modeling analysis was performed using an in-house code, which is available from the corresponding author upon request, and the resulting plasma parameters are available on Zenodo (https://doi.org/10.5281/zenodo.12802043).

Pitch angle distributions of ions and electrons

The pitch angle α is defined as the angle between a particle's velocity vector and the local magnetic field. For electrons, α values are provided in the JADE-E and JEDI-E datasets and are used directly. In contrast, ion pitch angles require additional calculation. The JADE-I dataset provides the local magnetic field vector and the look direction ($\boldsymbol{\theta}_\mathbf{l}$) for each measurement, allowing α to be computed as: $\alpha = \arccos(-\boldsymbol{\theta}_\mathbf{l} \cdot \mathbf{B}/|\mathbf{B}|)$. For low-energy ions, pitch angle distributions are influenced by plasma bulk velocity[55]. To minimize this bias, we restrict ion analysis to energies above 10 keV/q, where ion kinetic velocities significantly exceed bulk flow velocity. Once α is determined for each data point, the data are binned to obtain the pitch angle dependent flux spectra (J') by averaging over all data points (J):

$$J'(\alpha_m, E, t) = \frac{\sum_i J(\alpha_i, E, t)\left[\alpha_m - \Delta\alpha/2 < \alpha_i < \alpha_m + \Delta\alpha/2\right]}{\sum_i \left[\alpha_m - \Delta\alpha/2 < \alpha_i < \alpha_m + \Delta\alpha/2\right]} \quad (1)$$

where $\left[\alpha_m - \Delta\alpha/2,\ \alpha_m + \Delta\alpha/2\right]$ defines the m-th pitch angle bin with width $\Delta\alpha$. E and t denote energy level and time, respectively. The term $\left[\alpha_m - \Delta\alpha/2 < \alpha_i < \alpha_m + \Delta\alpha/2\right]$ equals 1 if true and 0 if false.

Determination of the LMN coordinate system

In the analysis of the ion diffusion region, we follow a similar approach to Eriksson et al.[40] to establish the local current sheet LMN coordinate system. Due to the limitations of single-spacecraft observations, the LMN system based on the cross-product normal is more robust than using the three eigenvectors of the Minimum Variance Analysis (MVA) of the magnetic field data, as illustrated in R. Wang et al.[41] and Knetter et al.[56]. The boundary-normal direction, $\mathbf{N}$, is defined as $\mathbf{B_1} \times \mathbf{B_2}/|\mathbf{B_1} \times \mathbf{B_2}|$, where $\mathbf{B_1}$ and $\mathbf{B_2}$ are magnetic field measurements adjacent to the candidate current sheet. In the reconnection event, the left boundary of the current sheet was identified at 02:02:56 UT, with $\mathbf{B_1}$ as the average magnetic field from three data points with a resolution of 1 s centered around this time. Similarly, $\mathbf{B_2}$ is the magnetic field observation at the right boundary, identified at 02:03:23 UT. The out-of-plane (or guide magnetic field) direction is $\mathbf{M} = \mathbf{N} \times \mathbf{L_{MVA}}/|\mathbf{N} \times \mathbf{L_{MVA}}|$, where $\mathbf{L_{MVA}}$ is the direction of the maximum magnetic field variance determined by MVA over the interval of current sheet observations (i.e., from 02:02:56 UT to 02:03:23 UT). Finally, the reconnection exhaust direction is obtained by completing the orthogonal system: $\mathbf{L} = \mathbf{M} \times \mathbf{N}$. In the MVA, the three eigenvalues are $\lambda =$ (458.14, 7.18, 0.66), and the large ratios between them confirm that $\mathbf{L_{MVA}}$ is well-defined. As a result, the determined vectors in the JSS coordinate system are organized into r, θ, and ϕ components: $\mathbf{L} =$ (−0.11, −0.85, 0.51), $\mathbf{M} =$ (0.22, 0.48, 0.85), and $\mathbf{N} =$ (−0.97, 0.20, 0.14). We compared $\mathbf{B_1}$ and $\mathbf{B_2}$ at different times relative to the current sheet, which always produce similar $\mathbf{M}$ and show similar Hall magnetic field patterns, which are crucial for identifying the ion diffusion region.

Estimations of key parameters in the magnetic reconnection event

Several key parameters are calculated to confirm the detection of the magnetic reconnection event and the diffusion region. First, to check the Walén relation, we calculate the Alfvén speed as $v_A = B/\sqrt{\mu_0 n m_i} =$ 91 km/s, where μ_0 is the vacuum permeability, $B =$ 41 nT is the average magnetic field intensity, $n =$ 4 cm^{-3} is the plasma density in the high density region, and $m_i =$ 24 amu is the average ion mass in the plasma disk. To check the energy conservation law, the input magnetic energy density is calculated as $E_b = B^2/(2\mu_0) = 6.7 \times 10^{-10}$ J/m^3. The gained kinetic energy density of the outflowing plasma is $E_k = 0.5 n m_i \triangle v^2 = 8.0 \times 10^{-10}$ J/m^3, where $\triangle v =$ 100 km/s is the increase in plasma flow velocity. To check the diffusion region scale, the ion inertial length is calculated as $d_i = c/\omega_{pi} =$ 370 km, where c is the speed of light. $\omega_{pi} = \sqrt{nZ^2e^2/(\epsilon_0 m_i)}$ is the ion plasma frequency, where ϵ_0 is the permittivity of free space and e is the elementary charge. $Z =$ 1.5 is the average charge state of ion plasma in the plasma disk[57]. Additionally, the bounce time of electron near the X-line of reconnection is estimated as

$t_b = 2\pi/\omega_b$. $\omega_b = \sqrt{eB_L v_e/m_e N}$ is electron bounce frequency[58], where $B_L = 30$ nT is the L-direction component of the magnetic field in the diffusion region, v_e is the electron velocity, m_e is the electron mass, and N=725 km is the current sheet thickness. For example, for a 1 keV electron, the bounce time is approximately 0.017 s.

Data availability

All the Juno observations used in this research are publicly available from the NASA Planetary Data System Plasma Interactions Node. The Juno JADE data are the level 3 version 04 data (https://doi.org/10.17189/1519715) from https://pds-ppi.igpp.ucla.edu/collection/JNO-J_SW-JAD-3-CALIBRATED-V1.0. Electron density and temperature are Juno JADE derived moments (level 5 version 01, https://doi.org/10.17189/2fch-6v84) from https://pds-ppi.igpp.ucla.edu/collection/JNO-J-JAD-5-MOMENTS-V1.0. The Juno magnetometer data are the level 3 version 01 data (https://doi.org/10.17189/1519711) from https://pds-ppi.igpp.ucla.edu/collection/JNO-J-3-FGM-CAL-V1.0. The Juno JEDI data are the level 3 version 01 data (https://doi.org/10.17189/1519713) from https://pds-ppi.igpp.ucla.edu/collection/JNO-J-JED-3-CDR-V1.0. The plasma bulk parameters are available at https://doi.org/10.5281/zenodo.12802043. Overview plots for each plasma disk crossing by Juno between 20 and 25 Jupiter radii are available at https://doi.org/10.5281/zenodo.17094279. Data generated in this study are available on Zenodo at https://doi.org/10.5281/zenodo.15786197. Source data are provided with this paper.

Code availability

The code used to reproduce the figures in this paper is available on Zenodo at https://doi.org/10.5281/zenodo.15786197. The code used for forward modeling analysis is an in-house code and is available from the corresponding author upon request.

References

1. Achilleos, N. et al. 1. Transport of mass, momentum and energy in planetary magnetodisc regions. *Space Sci. Rev.* **187**, 229–299 (2015).
2. Zhao, J. et al. Dayside magnetodisk reconnection in Jovian system: Galileo and Voyager observation. *J. Geophys. Res. Planets* **129**, e2023JE008240 (2024).
3. Louarn, P. et al. Magnetic reconnection and associated transient phenomena within the magnetospheres of Jupiter and Saturn. *Space Sci. Rev.* **187**, 181–227 (2015).
4. Vasyliunas, V. M. Plasma distribution and flow. *Phys. Jovian Magnetos.* **1**, 395–453 (1983).
5. Bagenal, F., Delamere, P. A. Flow of mass and energy in the magnetospheres of Jupiter and Saturn. *J. Geophys. Res. Space Phys.* **116**. https://doi.org/10.1029/2010JA016294 (2011).
6. Southwood, D. J. & Kivelson, M. G. Magnetospheric interchange instability. *J. Geophys. Res. Space Phys.* **92**, 109–116 (1987).
7. Kivelson, M. G., Southwood, D. J. Dynamical consequences of two modes of centrifugal instability in Jupiter's outer magnetosphere. *J. Geophys. Res. Space Phys.* **110**. https://doi.org/10.1029/2005JA011176 (2005).
8. Ma, X., Delamere, P. A. & Otto, A. Plasma transport driven by the Rayleigh-Taylor instability. *J. Geophys. Res. Space Phys.* **121**, 5260–5271 (2016).
9. Ma, X. et al. Flux tube entropy and specific entropy in Saturn's magnetosphere. *J. Geophys. Res. Space Phys.* **124**, 1593–1611 (2019).
10. Vogt, M. F., et al. Reconnection and flows in the Jovian magnetotail as inferred from magnetometer observations. *J. Geophys. Res. Space Phys.* **115**. https://doi.org/10.1029/2009JA015098 (2010).
11. Vogt, M. F. et al. Structure and statistical properties of plasmoids in Jupiter's magnetotail. *J. Geophys. Res. Space Phys.* **119**, 821–843 (2014).
12. Artemyev, A. V. et al. Juno observations of heavy ion energization during transient dipolarizations in Jupiter magnetotail. *J. Geophys. Res. Space Phys.* **125**, e2020JA027933 (2020).
13. Blöcker, A. et al. Dipolarization fronts in the Jovian magnetotail: Statistical survey of ion intensity variations using Juno observations. *J. Geophys. Res. Space Phys.* **128**, e2023JA031312 (2023).
14. Øieroset, M. et al. In situ detection of collisionless reconnection in the Earth's magnetotail. *Nature* **412**, 414–417 (2001).
15. Mozer, F. S., Bale, S. D. & Phan, T. D. Evidence of diffusion regions at a subsolar magnetopause crossing. *Phys. Rev. Lett.* **89**, 015002 (2002).
16. Birn, J. et al. Geospace Environmental Modeling (GEM) magnetic reconnection challenge. *J. Geophys. Res. Space Phys.* **106**, 3715–3719 (2001).
17. Shay, M. A. et al. Structure of the dissipation region during collisionless magnetic reconnection. *J. Geophys. Res. Space Phys.* **103**, 9165–9176 (1998).
18. Arridge, C. S. et al. Cassini in situ observations of long-duration magnetic reconnection in Saturn's magnetotail. *Nat. Phys.* **12**, 268–271 (2016).
19. Guo, R. L. et al. Rotationally driven magnetic reconnection in Saturn's dayside. *Nat. Astron.* **2**, 640–645 (2018).
20. Gao, J. W. et al. In situ observations of the ion diffusion region in the Venusian Magnetotail. *J. Geophys. Res. Space Phys.* **126**, e2020JA028547 (2021).
21. Wen, Y. et al. Multipoint observations of magnetic reconnection in the martian magnetotail triggered by an interplanetary magnetic field rotation. *Astrophys. J. Lett.* **982**, L42 (2025).
22. Connerney, J. E. P. et al. The Juno magnetic field investigation. *Space Sci. Rev.* **213**, 39–138 (2017).
23. Wang, J. Z. et al. Forward modeling of 3-d ion properties in Jupiter's magnetosphere using Juno/Jade-I data. *J. Geophys. Res. Space Phys.* **129**, e2023JA032218 (2024a).
24. Wang, J. Z. et al. Radial and vertical structures of plasma disk in Jupiter's middle magnetosphere. *J. Geophys. Res. Space Phys.* **129**, e2024JA032715 (2024b).
25. McComas, D. J. et al. The Jovian auroral distributions experiment (JADE) on the Juno mission to Jupiter. *Space Sci. Rev.* **213**, 547–643 (2017).
26. Joy, S. P. et al. Probabilistic models of the Jovian magnetopause and bow shock locations. *J. Geophys. Res. Space Phys.* **107**, SMP-17 (2002).
27. Connerney, J. E. P. et al. A new model of Jupiter's magnetic field from Juno's first nine orbits. *Geophys. Res. Lett.* **45**, 2590–2596 (2018).
28. Montgomery, J. et al. Investigating the occurrence of magnetic reconnection at Jupiter's dawn magnetopause during the Juno era. *Geophys. Res. Lett.* **49**, e2022GL099141 (2022).
29. Kacem, I. et al. Magnetic reconnection at a thin current sheet separating two interlaced flux tubes at the Earth's magnetopause. *J. Geophys. Res. Space Phys.* **123**, 1779–1793 (2018).
30. Sonnerup, B. Ö et al. Quality measure for the Walén relation. *J. Geophys. Res. Space Phys.* **123**, 9979–9990 (2018).
31. Kurth, W. et al. The Juno waves investigation. *Space Sci. Rev.* **213**, 347–392 (2017).
32. Dokgo, K. et al. High-frequency wave generation in magnetotail reconnection: Nonlinear harmonics of upper hybrid waves. *Geophys. Res. Lett.* **46**, 7873–7882 (2019).
33. Daly, A. et al. Statistical survey of interchange events in the Jovian magnetosphere using Juno observations. *Geophys. Res. Lett.* **51**, e2024GL110300 (2024).
34. Vogt, M. F. et al. Magnetotail reconnection at Jupiter: a survey of Juno magnetic field observations. *J. Geophys. Res. Space Phys.* **125**, e2019JA027486 (2020).
35. Mauk, B. H. et al. Storm-like dynamics of Jupiter's inner and middle magnetosphere. *J. Geophys. Res. Space Phys.* **104**, 22759–22778 (1999).

36. Øieroset, M. et al. MMS observations of large guide field symmetric reconnection between colliding reconnection jets at the center of a magnetic flux rope at the magnetopause. *Geophys. Res. Lett.* **43**, 5536–5544 (2016).
37. Burch, J. L. & Phan, T. D. Magnetic reconnection at the dayside magnetopause: advances with MMS. *Geophys. Res. Lett.* **43**, 8327–8338 (2016).
38. Alexandrova, A. et al. Two interacting X lines in magnetotail: evolution of collision between the counterstreaming jets. *Geophys. Res. Lett.* **43**, 7795–7803 (2016).
39. Qi, Y. et al. Temporal evolution of flux tube entanglement at the magnetopause as observed by the MMS satellites. *Geophys. Res. Lett.* **47**, e2020GL090314 (2020).
40. Eriksson, S. et al. Parker Solar Probe observations of magnetic reconnection exhausts in quiescent plasmas near the sun. *Astrophys. J.* **965**, 76 (2024).
41. Wang, R. et al. Solar wind current sheets: MVA inaccuracy and recommended single-spacecraft methodology. *J. Geophys. Res. Space Phys.* **129**, e2023JA032215 (2024).
42. Eastwood, J. P. et al. Asymmetry of the ion diffusion region Hall electric and magnetic fields during guide field reconnection: Observations and comparison with simulations. *Phys. Rev. Lett.* **104**, 205001 (2010).
43. Cassak, P. A., & Shay, M. A. Scaling of asymmetric magnetic reconnection: general theory and collisional simulations. *Phys. Plasmas*, **14**. https://doi.org/10.1063/1.2795630 (2007).
44. Pritchett, P. L. Collisionless magnetic reconnection in an asymmetric current sheet. *J. Geophys. Res. Space Phys.* **113**. https://doi.org/10.1029/2007JA012930 (2008).
45. Birn, J., Borovsky, J. E. and Hesse, M. Properties of asymmetric magnetic reconnection. *Phys. Plasmas*. **15**. https://doi.org/10.1063/1.2888491 (2008).
46. Mauk, B. H. et al. The Jupiter energetic particle detector instrument (JEDI) investigation for the Juno mission. *Space Sci. Rev.* **213**, 289–346 (2017).
47. Ma, Q. et al. Energetic electron distributions near the magnetic equator in the Jovian plasma sheet and outer radiation belt using Juno observations. *Geophys. Res. Lett.* **48**, e2021GL095833 (2021).
48. Xiong, Q. Y. et al. Statistic properties of electron energy enhancement during the inner electron diffusion region crossing. *J. Geophys. Res. Space Phys.* **127**, e2022JA030760 (2022).
49. Oka, M. et al. Particle acceleration by magnetic reconnection in geospace. *Space Sci. Rev.* **219**, 75 (2023).
50. Wang, C. Q. et al. First observation of electron rolling-pin distribution in Jupiter's magnetosphere. *Geophys. Res. Lett.* **51**, e2024GL108430 (2024).
51. Liu, Z. Y. et al. Juno observations of Jupiter's magnetodisk plasma: implications for equilibrium and dynamics. *J. Geophys. Res. Space Phys.* **129**, e2024JA032976 (2024).
52. Ferrière, K. Low-frequency waves and instabilities in collisionless plasmas. *Space Sci. Rev.* **122**, 247–253 (2006).
53. Egedal, J. et al. Evidence and theory for trapped electrons in guide field magnetotail reconnection. *J. Geophys. Res. Space Phys.* **113**, 12207 (2008).
54. Delamere, P. A., Bagenal, F., Steffl, A. Radial variations in the Io plasma torus during the Cassini era. *J. Geophys. Res. Space Phys.* **110**. https://doi.org/10.1029/2005JA011251 (2005).
55. Sarkango, Y. et al. Proton equatorial pitch angle distributions in Jupiter's inner magnetosphere. *Geophys. Res. Lett.* **50**, e2023GL104374 (2023).
56. Knetter, T., et al. Four-point discontinuity observations using Cluster magnetic field data: a statistical survey. *J. Geophys. Res. Space Phys.* **109**. https://doi.org/10.1029/2003JA010099 (2004).
57. Bagenal, F. et al. Survey of Galileo plasma observations in Jupiter's plasma sheet. *J. Geophys. Res. Planets* **121**, 871–894 (2016).
58. Norgren, C. et al. Electron and ion dynamics in reconnection diffusion regions. *Space Sci. Rev.* **221**, 1–73 (2025).

Acknowledgements

The authors would like to thank the Juno science team, without whose support this research would not be possible. This work was supported at the University of Colorado as a part of NASA's Juno mission funded by NASA through contract 699050X (F.B.).

Author contributions

Supervised by F.B., J.-Z.W. wrote the manuscript and performed the data analysis. S.E., R.E.E., F.B., and L.C.R. contributed to the interpretation of the reconnection event. S.E. contributed to the current sheet coordinate analysis. P.A.D. contributed to the flux tube interchange driven reconnection model. R.J.W. contributed to the generation of the JADE data. R.W.E., P.W.V., and F.A. contributed to building the JADE instrument, on which the study is based. R.J.W. and R.W.E. contributed to the JADE data analysis. All authors contributed to discussing the results and editing the manuscript.

Competing interests

The authors declare no competing interests.

Additional information

Supplementary information The online version contains supplementary material available at https://doi.org/10.1038/s41467-025-65981-9.

Correspondence and requests for materials should be addressed to Jian-zhao Wang.

Peer review information *Nature Communications* thanks Markku Alho and the other anonymous reviewers for their contribution to the peer review of this work. A peer review file is available.